

Nanodrop impact on solid surfaces

Joel Koplik* and Rui Zhang†

Benjamin Levich Institute and Department of Physics

City College of the City University of New York, New York, NY 10031

(Dated: August 24, 2012)

The impact of nanometer sized drops on solid surfaces is studied using molecular dynamics simulations. Equilibrated floating drops consisting of short chains of Lennard-Jones liquids with adjustable volatility are directed normally onto an atomistic solid surface where they are observed to bounce, stick, splash or disintegrate, depending on the initial velocity and the nature of the materials involved. Drops impacting at low velocity bounce from non-wetting surfaces but stick and subsequently spread slowly on wetting surfaces. Higher velocity impacts produce a prompt splash followed by disintegration of the drop, while at still higher velocity drops disintegrate immediately. The disintegration can be understood as either a loss of coherence of the liquid or as the result of a local temperature exceeding the liquid-vapor coexistence value. In contrast to macroscopic drops, the presence of vapor outside the drop does not effect the behavior in any significant way. Nonetheless, the transition between the splashing and bouncing/sticking regimes occur at Reynolds and Weber numbers similar to those found for larger drops.

* koplik@sci.ccny.cuny.edu

† ruizhang@ccny.cuny.edu

I. INTRODUCTION

The splashing of liquid drops on a solid surface has long been a subject of both visual appreciation [1] and quantitative fluid mechanical studies [2, 3]. Recent experiments [4] have reinvigorated this subject, by showing that removal of the vapor surrounding a drop suppresses splashing, an effect commonly associated with the presence of a lubrication layer of gas beneath an impacting drop, and a number of papers discuss splash modeling taking account of the gas. Recent examples, from which earlier literature may be traced, include [5–7]. Detailed flow measurements of splashing laboratory drops are challenging, due to the speed of the process and the small length scales involved, which motivates us to perform molecular dynamics simulations. Here, control of the materials and initial conditions is straightforward and configurational information and flow fields at fine spatial and temporal resolution are relatively easy to obtain. A particular advantage of this method is that the initial presence and distribution of vapor outside the drop may be altered at will. The price of high resolution and control is that only relatively small systems may be studied in this way, and we have considered drops roughly 12 nm in radius. Although many aspects of macroscopic fluid flows have been found to persist down to this scale, differences exist (see below), and we find that nanodrop impacts only partially agree with recent laboratory observations. In particular, the presence of vapor does not appear to be necessary for nanodrops to splash.

II. SIMULATION METHOD

The simulations employ standard classical molecular dynamics techniques [8, 9]. The drops are composed of small liquid molecules containing either two or four Lennard-Jones (LJ) atoms, bound into flexible linear chains by a FENE interaction [10]. The drops contain 157,126 atoms placed at the center of a box of dimensions $(X, Y, Z) = (300, 100, 300)\sigma$ and are initially equilibrated while floating freely using a Nosé-Hoover thermostat at temperature $T=0.8 \epsilon/k_B$. Here, ϵ and σ are the length and energy parameters in the LJ potential, and k_B is Boltzmann's constant. The characteristic time unit in the simulations is $\tau = \sigma(m/\epsilon)^{1/2}$ where m is the atomic mass. Representative physical values of these parameters are $\sigma \sim 0.34\text{nm}$ and $\tau \sim 2 \text{ ps}$. In the simulations, Newton's equations are integrated using a fifth-

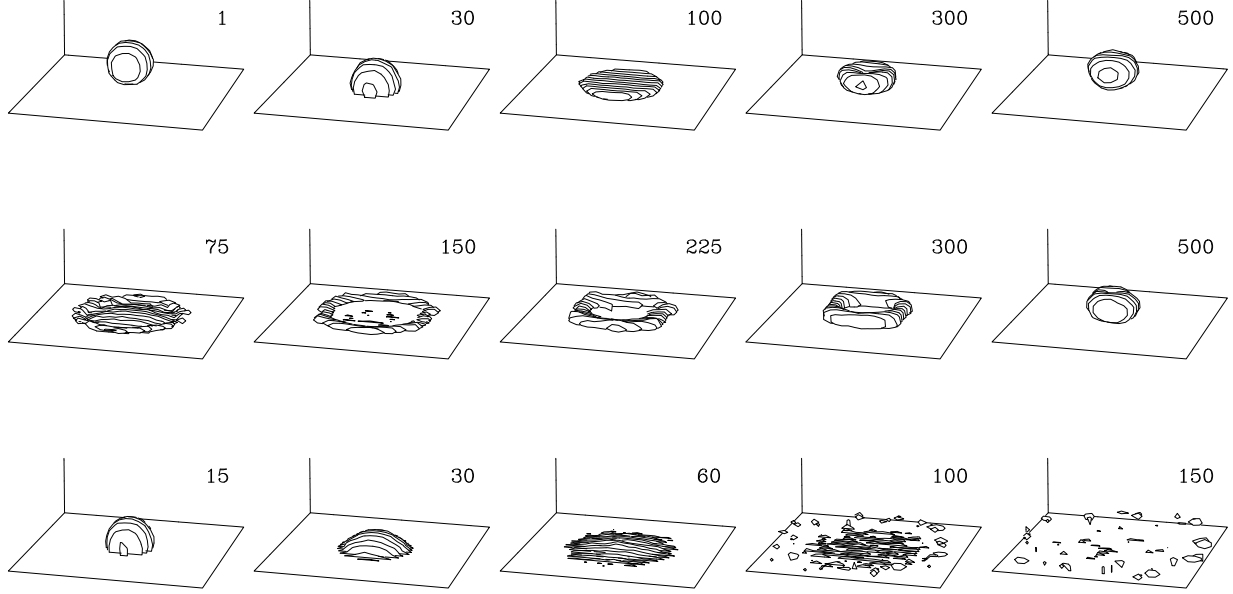


FIG. 1. Snapshots of the Impact of a non-volatile drop on a non-wetting solid surface, at velocities 1 (top row), 1.5 (middle row) and $2.0\sigma/\tau$ (bottom row). The plot depicts the mean interface of the drop at the indicated times.

order predictor-corrector method with a time step of 0.0005τ .

The dimer system forms a spherical drop of radius 36σ with an atomic (mass) density $\rho=0.80m\sigma^{-3}$, surrounded by vapor of atomic density $5\times 10^{-4}m\sigma^{-3}$. The “edge” of the drop is actually a sigmoidally-shaped transition region between liquid and vapor with a width of a few σ , and the ratio of vapor to liquid densities is about a half of that of air to water at room conditions. The tetramer system forms a similar drop of radius 35.8σ and density $\rho=0.86\ m\sigma^{-3}$ but in contrast to the dimers has very little vapor under these conditions, less than 1/10 the density of the dimer case. In addition, we have in some cases also considered two variant systems, one in which a drop of tetramer is surrounded by vapor of the dimer system, as a caricature of water drops in air, and the second a dimer system in which the vapor molecules are removed by hand at the moment when the drop is given its initial downward velocity. (We do not consider a monatomic liquid because its vapor pressure is so high as to obscure the shape of the interface after impact.) The simulation box is periodic in the transverse x and z directions while the bottom of the box has one layer of fcc cells of solid atoms, which are mobile but tethered to the lattice sites by stiff springs. The fluid atoms have a standard unit-strength LJ interaction with each other, while in most

	dimer	tetramer
μ ($m/\sigma\tau$)	2.80	3.42
γ (m/τ^2)	0.51	0.67
ρ ($m\sigma^{-3}$)	0.80	0.86
R (σ)	36.0	35.8

TABLE I. Physical properties of the drops.

u_0	dimer		tetramer	
	Re	We	Re	We
1.0	10.3	31.	9.0	46.0
1.5	15.5	127.	13.5	104.
2.0	41.2	226.	18.0	184.
3.0	31.0	552.	27.0	208.

TABLE II. Simulation parameters

cases the interaction between fluid and solid atoms has only a r^{-12} repulsive component, corresponding to a completely non-wetting system. We occasionally refer to a completely-wetting solid where the liquid-solid interaction has standard strength, but the effects of wettability and patterned surfaces are explored in more detail in subsequent paper. The combined liquid-vapor-solid system is equilibrated for 100τ , sufficient for the drop radii and densities to stabilize.

After equilibration the velocity of each atom in the drop is shifted by a negative constant in the vertical direction so as to translate the drop downward normally towards the solid surface. In the volatile case this additional velocity is smoothly turned off outside the interfacial region and the external vapor velocities are not shifted at all. In the remainder of the simulation the solid surface is held at constant temperature, but the temperature of the drop and vapor are allowed to vary. In Table I we give the viscosity μ and surface tension γ of the dimer and tetramer liquids used here, at the initial temperature of the simulations, along with the drop densities and radii. The viscosities and surface tensions were determined by standard methods [11], using independent simulations of Couette flow, and analysis of a periodic slab of liquid in contact with vapor, respectively. In Table II

we list the initial impact velocities u_0 and the corresponding values of the Reynolds and Weber numbers, $Re = \rho u_0 R / \mu$ and $We = \rho u_0^2 R / \gamma$. We have also simulated both lower (0.3) and higher (10.0) initial velocity impacts, but these do not exhibit any qualitatively different behavior. Given the fixed properties of the two liquids, the only remaining variable parameter is the initial velocity and We/Re^2 is a material constant.

Although the values of Re and We fall in a range suitable for comparison to laboratory experiments, one distinctly different property is the Mach number, $Ma = u_0/u_s$ where u_s is the sound speed. In the Appendix we present measurements of the sound speed in the two liquids. which gives an estimate $u_s \sim 5\sigma/\tau$. As a result the Mach number in these simulations is not negligible, ranging from 0.2 – 0.5. The underlying reason for high Ma in comparison to typical laboratory systems is that it is necessary to use relatively large velocities (typically 0.01 - 1.0 σ/τ) in molecular simulations to see any signal over the thermal fluctuation noise, whereas the thermal velocity is $O(1)$ in these units. However, we find that significant density variations appear only at the highest velocities studied here.

III. RESULTS

A. Shape and density

We first consider the non-volatile tetramer liquid impacting a non-wetting surface at different speeds. In Fig. 1 we show the evolution of the drop shape in terms of the “mean liquid-vapor interface,” the surface on which the fluid density is half of that in the original drop interior. In all cases, the drop is initially spherical and after contact continues to fall vertically and initially distorts into a hemisphere. At impact velocity 1.0 σ/τ the drop bounces, first spreading radially into a flat-topped lamella or pancake with maximum extension at about 100τ , and then curling up at the edges and beginning to withdraw while remaining in contact with the surface. Subsequently the drop lifts off the surface and continues to contract into a sphere, although the completion of the latter process requires several hundred τ beyond the last frame shown. The shape evolution of the drops is clearest in terms of density contours: using the centerline of the falling drop as the axis of a fixed cylindrical coordinate system, we average over azimuthal angle and measure the density of atoms as a function of height and radius, averaged over 10τ intervals. A selection of the

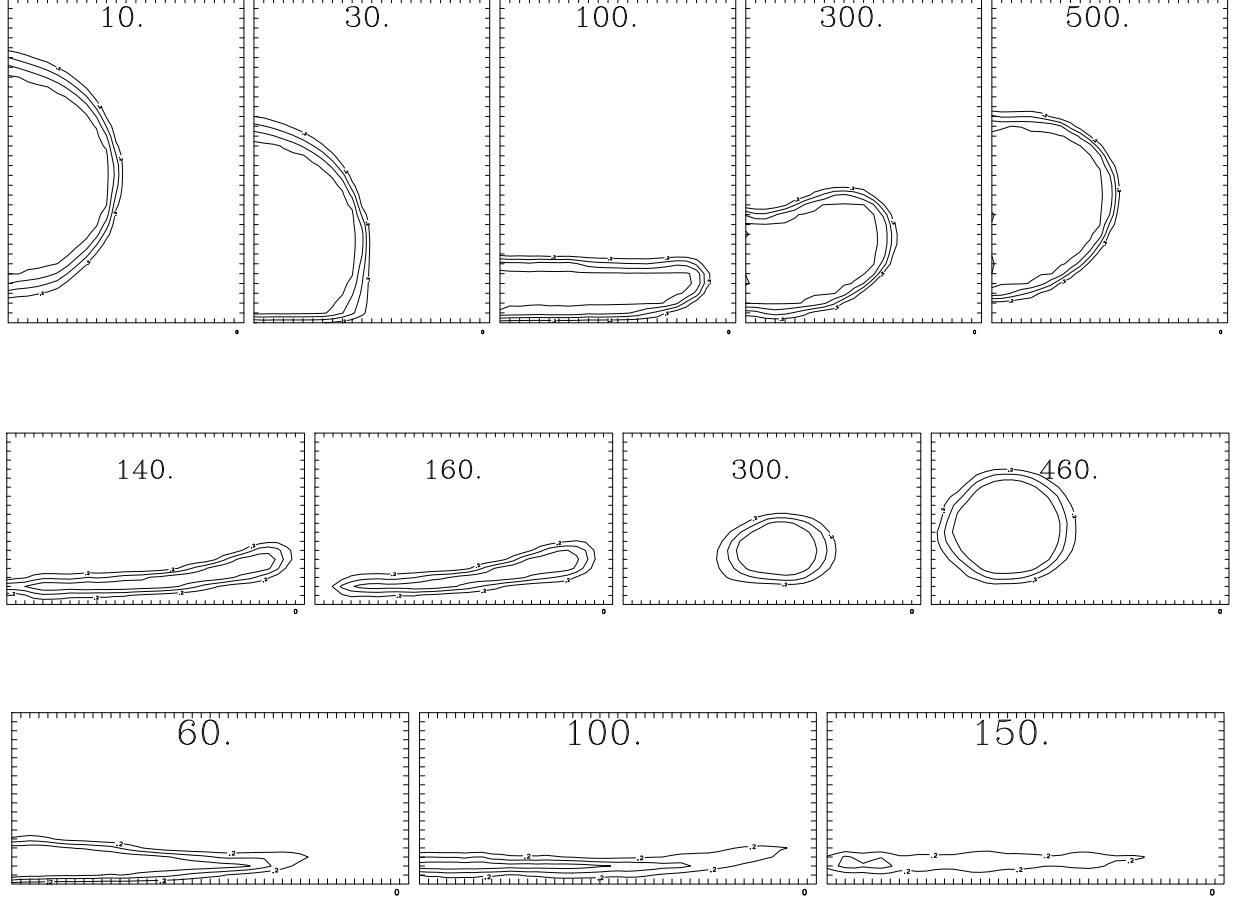


FIG. 2. Density contours for impacting drops on non-wetting surfaces, averaged over the 10 τ interval preceding the indicated time, in cylindrical coordinates relative to the impact axis. The initial density at the center of the drop is $0.86 m\sigma^{-3}$, the outer contour in each frame represents density 0.2, and the inner contours are spaced by 0.2. Top to bottom: impact velocities 1.0, 1.5 and 2.0 σ/τ .

resulting density contours corresponding to the surface plots at the same three impact velocities are given in Fig. 2. In the low-velocity bounce, the contact angle first decreases from 180° at contact to 90° at 30τ as seen previously, to roughly 45° at time 50τ (not shown). Afterwards the rim of the lamella rises and the angle increases as the drop contracts. The curvature at the top of the drop is initially positive and decreases until the top is roughly flat at maximum lateral extension, then goes negative as the drop's edges contract and rise, and eventually returns to positive as the drop rises and slowly returns to a sphere.

At velocity $1.5 \sigma/\tau$ the drop again bounces, but at intermediate times develops a remarkable transient toroidal shape before surface tension acts to restore it to a sphere: see the

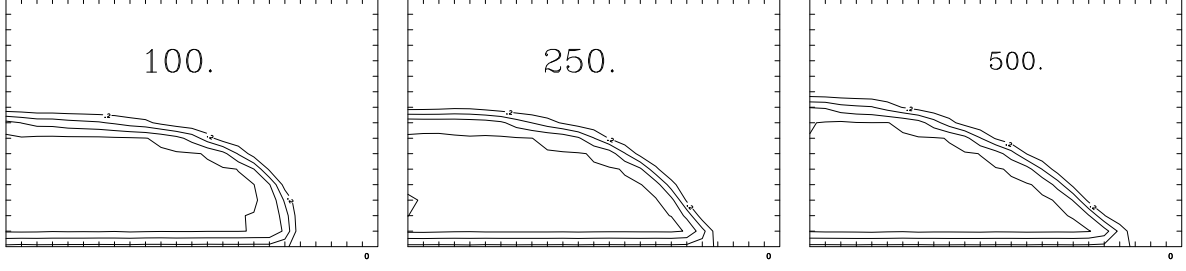


FIG. 3. Density contours for a drop impacting a completely wetting surface at impact velocity $1.0 \sigma/\tau$. The format is identical to Fig. 2.

middle rows of Figs. 1 and 2. The density contours are similar to the lower-velocity case up to time 100τ but then show the drop continuing to spread and a hole opening at the drop center. In comparison to the lower-velocity case, after impact here the spreading lamella moves outwards so rapidly as to evacuate the central region about the impact point. Aside from its transience, the toroidal state is somewhat special since it only appears in a narrow velocity range for tetramer drops and was not observed in simulations in the dimer systems. An intuitive explanation is that a tetramer liquid is more coherent and less extendible than monomer or dimer liquids because the longer chains tend to intermingle. When stretched outwards by inertia, the drop resists indefinite thinning and disintegration by rupturing to form a dense ring.

At still higher impact velocity, $2.0 \sigma/\tau$, the drop again initially evolves into a hemisphere and then again into a lamella, which is distinctly thinner than those at lower velocities. The lamella spreads but its thickness and density decrease with time, and instead of contracting it develops a splash and eventually evaporates as the drop disintegrates – see the bottom rows of Figs. 1 and 2. The mean surface falls apart into isolated liquid regions, meaning that lower-density fluid fills the simulation region. A liquid jet is in fact emitted from the edge of the lamella (a prompt splash) around time 30τ , but this is a low-density phenomenon not evident in these plots and will be illustrated below. At even higher velocity, $3.0 \sigma/\tau$, the surface and density plots are similar (on a faster time scale) but the drop seems to disintegrate without a distinct splash phase. To elucidate splashing, and to compare the impact behavior of different liquids, in the following subsection we employ an alternate display of the drops with molecular resolution.

In the bouncing cases, note that the thickness of the interfacial region – the width of the

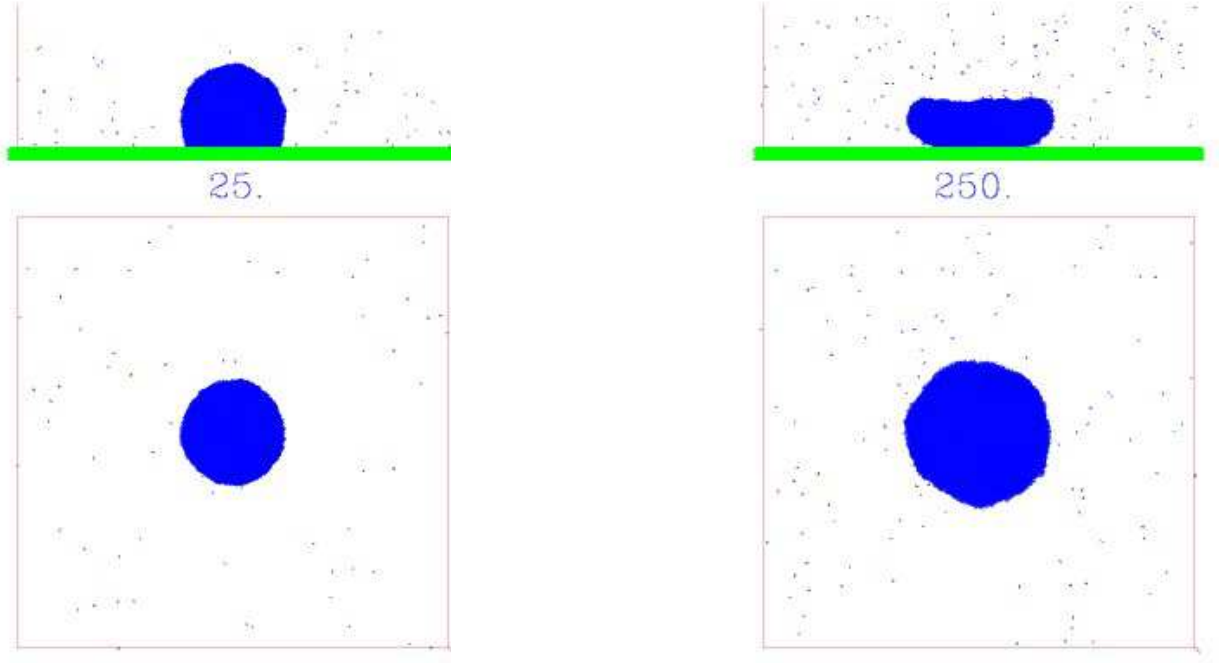


FIG. 4. Simultaneous top and side molecular views of an impacting tetramer drop at velocity $1.0 \sigma/\tau$ at the time indicated. Each molecule is displayed as the three (blue) bonds joining the atoms and the horizontal (green) band indicates the positions of solid atoms. Left: slightly after impact, Right: during recoil.

set of parallel curves enclosing the drop – does not vary substantially during the bounce. This indicates that the interface does not broaden and that there is little density variation in the interior of the drop, or in other words that the drop is approximately incompressible in this case. The interfacial thickness here is slightly larger than that of a drop at rest, because the drop is in motion during the averaging time interval. The density fluctuates weakly during the bounce, but the peak value (roughly 10% above the value at rest) occurs only briefly and locally, just after contact in the hemispherical state. In the splash regime the situation is quite different. There is no evidence for a constant density interior during and after impact, but rather the density varies throughout the drop's interior and furthermore decreases systematically during the splash and disintegration as more and more vapor appears.

The difference in drop behavior between wetting and non-wetting surfaces is indicated in Fig. 3. At time 100τ , the spreading lamella on a *completely wetting* surface has ceased its

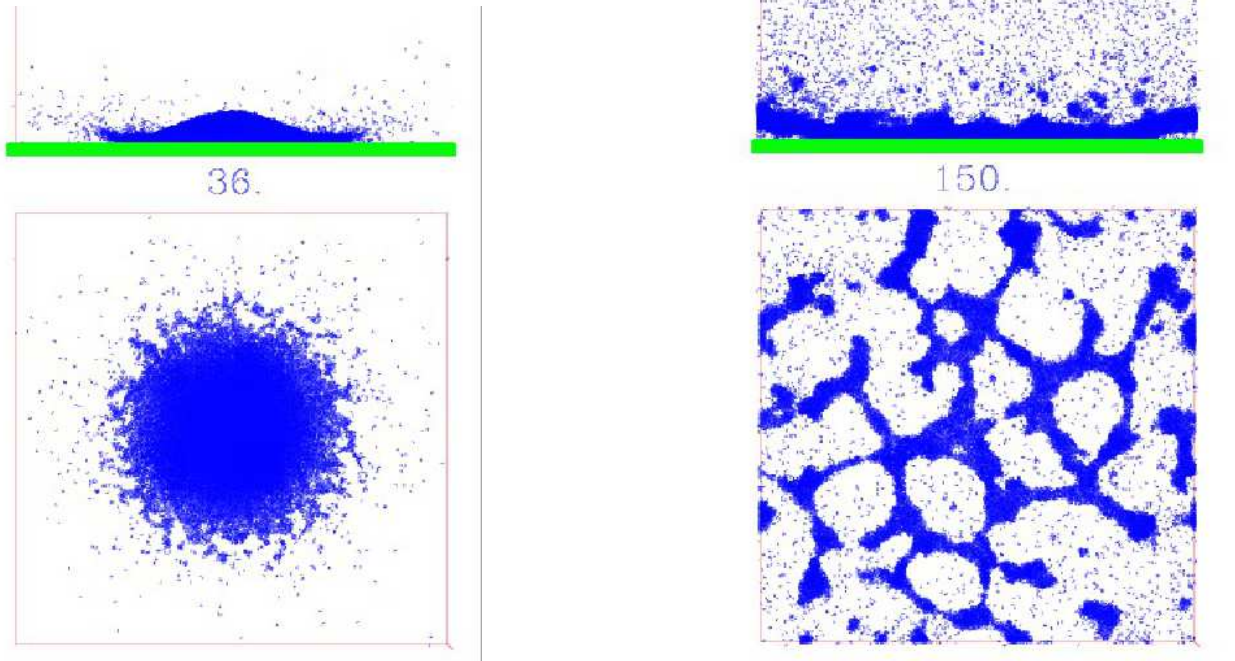


FIG. 5. Simultaneous top and side molecular views of an impacting tetramer drop at velocity $2.0 \sigma/\tau$. Each molecule is displayed as the three bonds joining the atoms. Left: during the splash phase, Right: at the end of the simulation.

rapid outward motion, and its tip has a downward curvature and a dynamic contact angle around 90° . At later times, the drop continues to spread due to capillary forces, but this is a much slower process than inertially-driven spreading, and even after 500τ little further outward motion has occurred. In contrast, on the non-wetting surface in Fig. 2, in the top row at time 100τ the tip of the lamella is detached from the surface with an upwards curvature and a dynamic contact angle closer to 180° .

B. Molecular detail

The distinction between the slow and fast impact cases and the effects of external vapor are most evident when individual molecular positions are displayed. Figure 4 shows a non-volatile bouncing drop in simultaneous top and side views, at early and late times after impact. Some individual vapor molecules are visible, but those inside the liquid are dense enough to uniformly fill the interior. The impact has slightly increased the amount of vapor but the liquid is quite coherent and the liquid-vapor interface and contact angle are well-

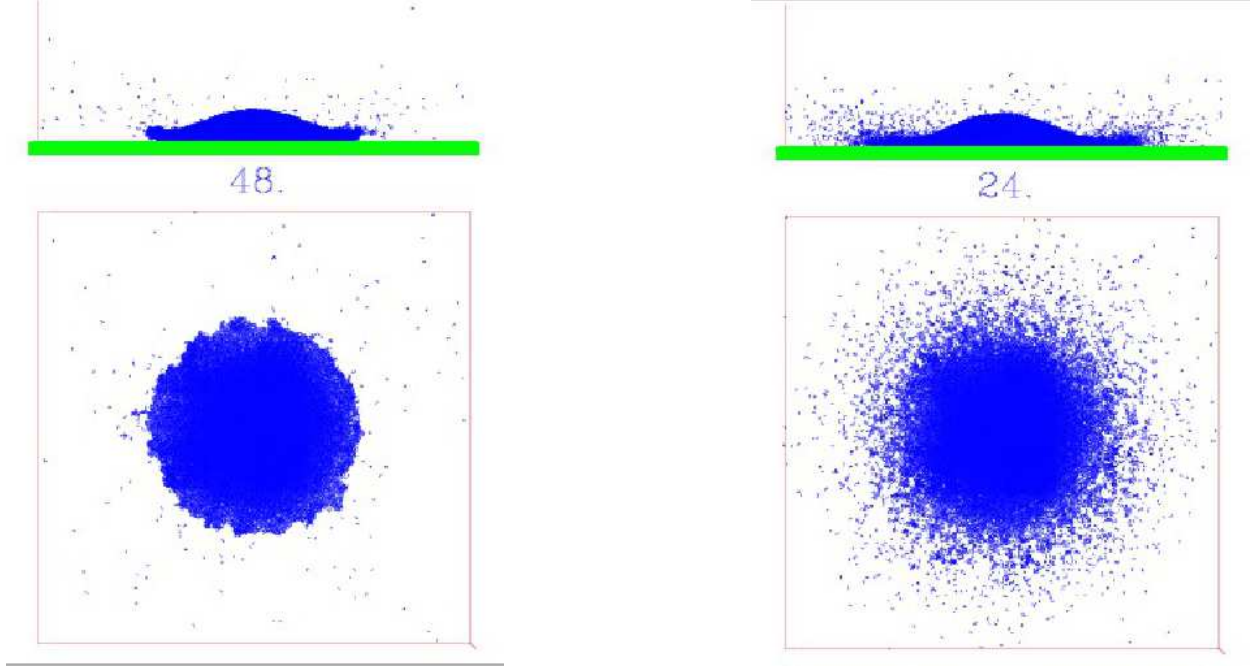


FIG. 6. Molecular views for comparison with Fig. 5 at 36τ . Left: tetramer drop at velocity $1.5\sigma/\tau$ at time 48τ , Right: tetramer drop at velocity $3.0\sigma/\tau$ at time 24τ .

defined. Hence, the mean interface and density plots above accurately capture the shape evolution of the drop. At twice the impact velocity, however, we see in Fig 5 that as the liquid spreads on the surface, a significant number of molecules are emitted into the vapor from the drop rim region. This is an example of a prompt splash: at time 36τ there is a crown-like rim rising above the surface and droplets breaking off at roughly regular angular spacing around the edge. Subsequently, the crown collapses as the drop evolves into a single pancake-like lamella which continues to spread but becomes inhomogeneous and develops holes, meanwhile steadily emitting vapor from its entire surface. Eventually, the liquid is reduced to a fragmentary pattern resembling spinodal decomposition, while enough vapor is produced to almost uniformly fill the simulation box. If the surface is completely wetting rather than repulsive, the corresponding molecular views at this impact velocity are similar through time 40τ or so but afterwards, while continuing to emit vapor, the lamella persists throughout the simulation as a well-defined thin disc or puddle which does not disintegrate.

The splashing state should be distinguished from drop disintegration, which occurs at still higher impact velocities. In Fig. 6 we show comparison snapshots of non-volatile impacts

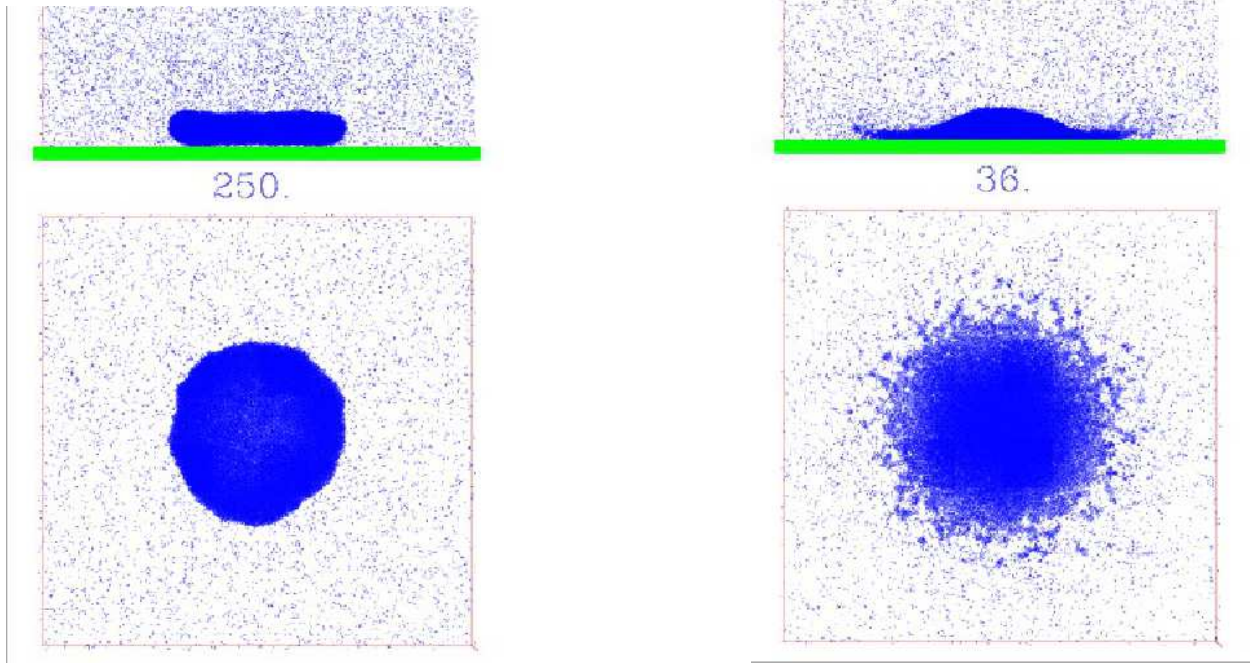


FIG. 7. Molecular views of an impacting dimer drop at velocity 1.0 (left) and 2.0 σ/τ (right), at the same times as for the tetramer drops in Figs.4,5.

at both lower and higher impact velocities at times corresponding to the same displacement $u_0 t$ as Fig. 5 at time 36 τ : $u_0 = 1.5 \sigma/\tau$ at $t = 48 \tau$ and $u_0 = 3 \sigma/\tau$ at $t = 24 \tau$. The slower case – the toroidal bounce – has a slightly irregular rim but no significant vapor emission as the lamella spreads. In the higher-velocity case, vapor is emitted from the entire lamella while the edge of the rim has a radially-decreasing density with little angular variation. The final state in this case (not shown) has a few irregular droplets on the surface and otherwise a dense fluid filling the box.

A key result of this paper is that this behavior is generic: the choice of molecular liquid and the presence or absence of surrounding vapor does not qualitatively effect the dynamics of nano-sized drop impacts. This conclusion is based on repeating these simulations with dimer liquids, with vapor present initially or not, and mixed tetramer-liquid/dimer-vapor drops with the same initial radius and impact velocities as those above. In all cases the mean-surface plots and density fields are very similar to those of tetramers and the only distinction is in the amount of vapor present after impact. For example, in Fig. 7 we display molecular snapshots of the dimer liquid at impact velocities 1.0 and 2.0 σ/τ at two of the

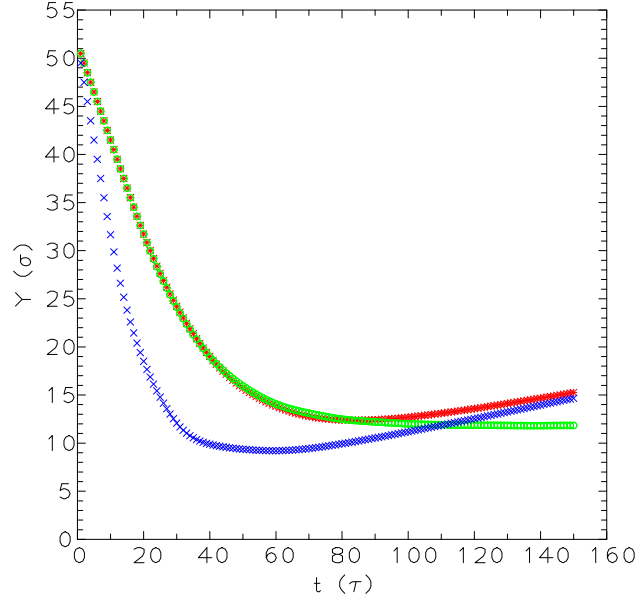


FIG. 8. Variation of the height of the center of mass of the fluid (liquid plus vapor) as a function of time. Initial velocity 1.0 (*), and 2.0 σ/τ (x) on a non-wetting surface and velocity 1.0 σ/τ (o) on a wetting surface.

same times as the tetramer simulations shown in Figs. 4b and 5a, respectively. In the first case, the drop is bouncing and has a well-defined and relatively smooth interface, with rather more vapor outside the drop. In the second frame the dimer drop is disintegrating in essentially the same way as the tetramer, and the vapor molecules are simply floating in the background.

Of course, variation of the liquid properties does change the Reynolds and Weber numbers for impact at a given velocity, and strictly speaking we should compare the different liquids by matching these quantities. In the examples above, the operating conditions were well inside the bounce and splash regimes, respectively, and the distinction was not crucial, but a difference does occur near the transition values. At velocity 1.5 σ/τ for example, the tetramer drop bounces (via the toroidal intermediate state shown in Fig. 1) but a dimer drop at the same velocity is found to simply splash. The dimer has higher Reynolds and Weber numbers and this behavior is still consistent with a critical Weber number $O(100)$ dividing the bouncing and splashing regimes. The experimental transition Weber number is rather higher than this, $O(500)$, which is one reason we speak of disintegration rather than splash – see below.

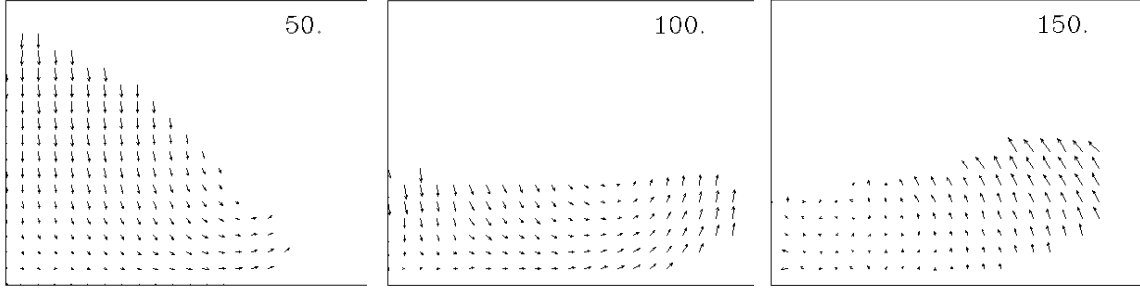


FIG. 9. Cylindrically averaged velocity field for a non-volatile drop impacting a surface at $u_0=1.0$ σ/τ . Each arrow represents the velocity averaged over a $3\sigma \times 3\sigma \times 360^\circ$ spatial bin and a 10τ time interval. The maximum velocity (longest arrow) in each frame is 0.94, 0.24 and 0.13 σ/τ , respectively.

The insensitivity to vapor is in contrast to the behavior of larger, millimeter-sized drops, where vapor appears to form a lubrication layer which causes a splash at sufficiently high velocity. The key difference is that although the vapor density in these simulations is similar to room conditions, the amount of vapor lying beneath a falling 12 nm drop is very small - tens of molecules - and insufficient to show any significant hydrodynamic behavior. When a drop impacts the surface, these few molecules are either adsorbed into the drop or pushed aside but do not effect its behavior. In further support of this conclusion, we have carried out two types of modified simulation. First, we simulated the impact of dimer drops in which either a fraction or all of the vapor molecules are deleted at the instant the drop is set into motion: there is no significant change in the splash. Second, in a complementary simulation, we surrounded a tetramer drop with dimer vapor before directing it downward. While the shape of the drop is slightly altered, Again there was no significant change in comparison to the original system.

C. Flow fields

The overall motion of the drop relative to the surface is not completely clear in the preceding figures, but may be shown by plotting the height of the center of the drop (more precisely, $Y(t)$, the y -coordinate of the center of mass of the fluid atoms) as a function of time. The result for tetramer drops is shown in Fig. 8: a V-shaped curve when the drop

bounces on a non-wetting surface and an L-shaped curve when the drop sticks to a wetting surface. The curve is always asymmetric because energy is adsorbed by the (thermostated) wall atoms during impact and spreading. A drop which splashes and then disintegrates also shows a nearly V-shaped variation, corresponding to the liquid drop moving downwards with the initial velocity followed by a smooth rise of the center of mass when its fragments rebound upwards off the surface. Once again, the corresponding curves for dimer drops are quite similar.

In addition to the density field shown above, we have attempted to measure two-dimensional fluid velocity and stress fields inside the drop. As an example, the cylindrically-averaged velocity field for a non-volatile drop impacting at $1.0 \sigma/\tau$ is shown in Fig. 9. At 50τ there is a roughly hyperbolic flow in which the original bottom of the drop is forced outwards while the upper half is still moving downwards. The radially outwards flow produces the spreading lamella, but at 100τ the radial motion at the edge of the rim has ceased and the rim is bending upwards, while the top of the drop continues to fall, and at 150τ the velocities are very small in the center of the drop while a faster contraction to a sphere is underway at the rim. The same sequence is observed for all bouncing drop cases, whereas when the surface is wetting the velocities simply decay to small random fluctuations when the initial rapid-spreading stage ends. In splashes or disintegrations, the velocity field is simply radially outwards at later times before decaying away. In these figures the vapor region is not shown because it contains too few molecules for averaging to produce a robust signal above the statistical fluctuations.

The pressure contours are similar in overall shape to the density field, meaning there is a pressure where there is a (dense) liquid, and beyond this the pressure is high at the wall due to impact. It is difficult to go beyond these qualitative statements here because of numerical imprecision. The shear stress is simply too noisy to resolve a signal above the fluctuations here. Generally, the stress tensor fluctuates strongly in molecular dynamics simulations, because it directly involves the inter-atomic force, which is a rapidly varying function of position. The use of long intervals of slowly-varying behavior for time-averaging or large homogeneous regions for spatial averaging can produce a robust signal, but these are absent in this problem. We have attempted to average the results over a modest statistical ensemble (of five realizations) to no avail. Presumably a much larger drop or much slower velocity would be required for precise stress measurements.

IV. DISCUSSION

These results indicate that splashing nanodrops differ from their larger-sized counterparts in (at least) two significant ways. First, the vapor surrounding a drop does not control the occurrence of splashes, basically because even though its density is comparable to laboratory values there are too few vapor molecules beneath a nano-sized drop to have any significant effect. In contrast, a macroscopic drop falling through an appreciable distance can trap a continuum air film beneath itself, which will build into a pressurized lubrication layer as the drop nears the surface, which in turn can exert enough shear stress on the bottom of the drop to deform it. Here we have only tens of molecules and no real film. The second difference is in the nature of the splash itself - at high velocities the edge of a nanodrop deformed by rapid impact appears to spew out molecules and disintegrate, and eventually the entire drop seems to fall apart. In contrast, macroscopic drops have enough molecules to retain their identity as dense liquids even after substantial deformation and stretching of the liquid-vapor interface, and even in such dramatic processes as crown formation the rim of the drop is still just a liquid sheet with bulbous protuberance at its edge.

One reason for the different structure in the final state of nanodrop splashes is volume - there are too few molecules available to populate all of the fine liquid details of a continuum splashing drop. A second reason is related to the high molecular speeds $u_0 \sim 1.0 \sigma/\tau \sim 100\text{m/s}$ necessary for a nano-sized drop to reach Reynolds and Weber numbers $O(100)$. In confined flows such velocities are not problematic, providing that the results are understood in terms of the appropriate dimensionless velocity *gradient*. if the Deborah or Weissenberg number is small one is simulating a Newtonian fluid and otherwise non-Newtonian behavior is expected. When a liquid-vapor interface is strongly deformed, however, there is the issue of coherence - holding the liquid together. Some insight into the lack of liquid coherence in the high-velocity impacts here comes from simple energetics: when the drop is at rest the potential energy per atom due to the LJ interaction is measured here to be -1.35ϵ and -1.48ϵ , respectively, in the dimer and tetramer cases. Since the kinetic energy per atom is $\frac{3}{2}k_B T = 1.2\epsilon$, the average energy per atom is only slightly negative, and since the interatomic potential vanishes outside a cutoff, in a sense the liquid is loosely bound. The kinetic energy is significantly increased by the initial velocity, nominally by 4.5ϵ in the fastest case above, and on impact the outward motion produces large velocity gradients and therefore large

relative kinetic energies of interacting pairs of molecules, which may then become unbound. Laboratory drops do not have so high an impact velocity and this effect is absent. This argument is not precise enough to accurately predict the transition velocity in nanodrop splashing, it is consistent with the observed transition velocity of about $1.5 \sigma/\tau$ and it does help explain the nature of the final state.

An alternative way of thinking about drop disintegration is in terms of temperature. In the low impact velocity case, the drop is initialized at $T=0.8 \epsilon/k_B$, which does not change when the drop is translated as a body (temperature is proportional to the mean-square velocity *fluctuation* about the mean), but the impact produces non-uniform velocity and temperature fields. At lower impact velocities the local temperature at the edge of the drop varies from 0.8 to 1.0, but in the higher velocity impact values above 2 occur. The point is that the latter values are above the critical temperature for the liquids simulated here, and since there is no distinction between liquid and vapor phases the drop is evaporating. Admittedly, the phase coexistence curve is directly meaningful only for homogeneous systems in equilibrium, but it does provide some qualitative insight. For a pure monatomic LJ fluid the critical temperature is known to be $1.1 \epsilon/k_B$ [12], but the molecular binding is expected to change the value. While we have not attempted to determine the full phase diagram, we have estimated the maximum temperature for phase coexistence at the densities of the present simulations by placing the equilibrated drop plus vapor molecular configurations in a periodic box of the same dimensions used in the impact calculations and observing the behavior at various temperatures. The result is that dimer drops evaporate at $T \simeq 1.1$ and tetramers at $T \simeq 1.4\epsilon/k_B$, and since we observe that these temperatures are exceeded on fast impact, we could qualitatively describe the drop disintegration seen here as rapid evaporation.

ACKNOWLEDGMENTS

We thank M. Brenner, S. Nagel and T. Witten for helpful discussions.

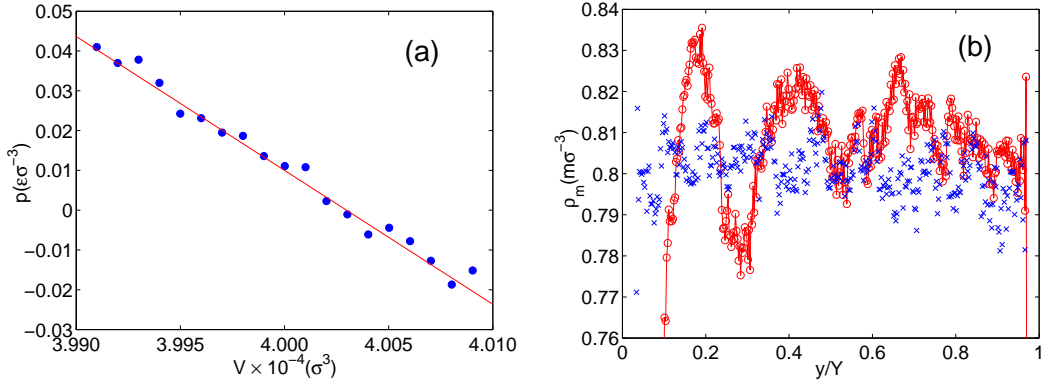


FIG. 10. (a) p - V diagram for dimers; points (blue) are simulation results and the line (red) is a fit. (b) Density profile produced by an oscillating wall: \circ oscillating wall, \times stationary wall.

Appendix A: Sound Speed

The sound speed is given generally by

$$u_s^2 = \left(\frac{\partial p}{\partial \rho} \right)_S = -\frac{V}{\rho} \left(\frac{\partial p}{\partial V} \right)_S,$$

where p and ρ are the pressure and mass density of the medium, respectively, where M is the atomic mass. The second form is useful in MD calculations, where it can be implemented by a sequence of NVT simulations in which the volume V is slowly varied while the constant entropy (S) constraint is satisfied by isolating the system thermally so that there is no heat flux. We first equilibrate a system of 16,000 dimer molecules in a periodic cube of side 34.2σ at temperature $0.8 \epsilon/k_B$ and density either slightly above or slightly below the target value $0.8 m\sigma^{-3}$. The volume is then either decreased or increased by 0.5% over a 400τ time interval, approximately an adiabatic variation in volume, so as to bracket the target density. The resulting pressure variation is shown in Fig. 10a, from which the slope of the linear least-squares fit gives $u_s = (4.1 \pm 0.1)\sigma/\tau$.

As a check on the result we use a second method: direct simulation of a sound wave. In this case we place a dimer liquid at the desired density in a rectangular simulation box of dimensions $(X, Y, Z) = (20.5, 215.5, 20.5)\sigma$, bounded by two solid walls in the (long) y -direction. After equilibration, one wall is rigidly oscillated in y at frequency $\omega = 0.6\tau^{-1}$ and amplitude σ . The opposite wall is fixed in place and thermostatted to adsorb the energy flux resulting from the oscillation. After a transient period, we observe a traveling

wave of spatial variation in density, depicted at one time in Fig. 10b. For reference, the density variation due to the oscillation is compared with that resulting from equilibrium fluctuations in the same fluid in a fixed volume. A clear signal is present near the moving wall, although the wave decays near the fixed wall due to energy adsorption there. From the spatial variation of density a wavelength can be extracted and, given the frequency, we find $u_s = (4.8 \pm 0.3)\sigma/\tau$. The two methods are in qualitative agreement, but we consider the first to be more reliable. Some deficiencies of the second method are (1) the temperature of the liquid is not controlled, (2) we have not taken account of any reflected wave, and (3) a rather high frequency is needed in order to have a wavelength well below the size of the simulation box.

liquid	$\rho \text{ (} m\sigma^{-3} \text{)}$	Method I	Method II
monomer	0.8	5.0 ± 0.1	5.7 ± 0.6
dimer	0.8	4.1 ± 0.1	4.8 ± 0.3
tetramer	0.86	4.8 ± 0.2	5.5 ± 0.4

TABLE III. Measurements of the speed of sound at $T = 0.8\epsilon/k_B$. Method I is based on the definition and Method II involves the direct simulation of sound waves.

The measurements were repeated for a monomer Lennard-Jones fluid as well as the tetramer fluid studied in the paper, and the results are summarized in Table III. The point of the monomer measurement is that this simulated material is a reasonable approximation to liquid Argon, whose sound speed has been measured experimentally to be 853m/s at 44.4MHz and 85K and atmospheric pressure [13], close to the simulation result for Method I. The fact that the sound speed in dimer liquids is lower than in monomer liquids is consistent in trend with ideal gas theory where $u_s = (\gamma k_B T/m)^{1/2}$: the adiabatic index γ is lower for dimers than monomers.

-
- [1] A. M. Worthington, *A Study of Splashes* (Longmans, Green, London, 1908).
 - [2] M. Rein, Phenomena of liquid drop impact on solid and liquid surfaces, *Fluid. Dyn. Res.* **12**, 61-93 (1993).
 - [3] A. L. Yarin, Drop impact dynamics: splashing, spreading, receding, bouncing, . . . , *Annu. Rev. Fluid. Mech.* **38**, 159-192 (2006).
 - [4] L. Xu, W. W. Zhang and S. R. Nagle, Drop splashing on a dry smooth surface, *Phys. Rev. Lett.* **94**, 184505 (2005).
 - [5] M. Mani, S. Mandre and M. P. Brenner, Events before droplet splashing on a solid surface, *J. Fluid Mech.* **647**, 163-185 (2010).
 - [6] P.D.Hicks and R. Purvis, Air cushioning and bubble entrapment in three-dimensional droplet impacts, *J. Fluid Mech.* **649**, 135-163 (2010).
 - [7] L. Duchemin and C. Josserand, Curvature singularity and film-skating during drop impact, *Phys. Fluids* **23**, 091701 (2011).
 - [8] M. P. Allen and D. J. Tildesley, *Computer Simulation of Liquids* (Clarendon Press, Oxford, 1987).
 - [9] D. Frenkel and B. Smit, *Understanding Molecular Simulation*, 2nd ed. (Academic, San Diego, 2002).
 - [10] K. Kremer and G. S. Grest, Molecular dynamics simulation for polymers in the presence of a heat bath, *Phys. Rev. A* **36**, 3628-31 (1986).
 - [11] J. Koplik and J. R. Banavar, Continuum deductions from molecular hydrodynamics, *Annu. Rev. Fluid Mech.* **27**, 257-92 (1995).
 - [12] H. Watanabe, N. Ito and C.-K. Hu, Phase diagram and universality of the Lennard-Jones gas-liquid system, *J. Chem. Phys.* **136**, 204102 (2012).
 - [13] D. E. Gray, ed., *American Institute of Physics Handbook of Physics*, 3rd. ed. (McGraw-Hill, New York, 1972).